Artificial Muscle Actuator Based on the Synthetic Elastomer

Nguyen Huu Chuc, Ja Choon Koo, Young Kwan Lee, Jae Do Nam and Hyouk Ryeol Choi*

Abstract: In this paper, we present an artificial muscle actuator producing rectilinear motion, called the Tube–Spring–Actuator (TSA). The TSA is supposed to be a prospective substitute in areas requiring macro forces such as robotics. It is simply configured from a synthetic elastomer tube with an inserted spring. The design of the TSA is described in detail and its analysis is conducted to investigate the characteristics of the actuator based on the derived model. In addition, the performance of the proposed actuator is tested via experiments.

Keywords: Artificial muscle actuator, EAP, synthetic elastomer.

1. INTRODUCTION

Recently, polymers have been emerging as substitutes for existing actuators such as electromagnetic motors, piezo actuators, etc. Up until now, there have been a wide variety of polymeric materials applicable to actuation as well as sensing. The most promising ones among them are the ElectroActive Polymer (EAP), Ionic Polymer Metal Composites (IPMC), conducting polymer, polymer gel, dielectric elastomer (DE) and piezo electric polymer [1]. In general, EAPs are classified into two groups, including ionic and non-ionic EAPs, depending on the physics of actuation. Presently, actuator technologies employing non-ionic EAPs such as the dielectric elastomer or piezo electric polymer have matured up to practical applications, though the other polymers also have a good potential of being implemented for practical use in the near future. Dielectric elastomers, which are one of the most feasible actuation materials because of their large deformation and force, are easily found at a moderate cost. There are numerous dielectric elastomers commercially available such as silicone, polyurethane, acrylic elastomer, etc. [2,3].

Actuators made from the dielectric elastomer have broad applications in robots, micro/milli devices, etc. So far, many configurations of actuators have been proposed such as the planar, tube, roll extender, diaphragm and bender actuator [4-10]. Among them the roll actuator was demonstrated to provide large strain as well as macro force [4,9]. Carpi *et al.* presented a new contractile linear actuator called the helical dielectric elastomer for actuating a Martian jumping rover, the eyeballs of an android robotic face and the anthropomorphic skeleton of an upper limb [5]. Wingert *et al.* proposed the design of a binary actuator with the dielectric elastomer [10].

Recently, we have developed a new material called synthetic elastomer whose properties, such as the mechanical properties, electrical properties as well as electromechanical properties, can be adjusted according to the requirements of the applications [11]. In this paper, we present an artificial muscle actuator based on the synthetic elastomer, which is able to provide rectilinear motion and is known as the tube-spring-actuator (TSA). The TSA is configured with a spring and a tube that is fabricated from the synthetic elastomer. The spring is inserted inside the cylindrical actuator after being compressed and it generates rectilinear motion according to the input voltage. A comprehensive description on the design, analysis, and fabrication are given, and the synthetic elastomer's performances are experimentally evaluated in this paper.

The present article is organized as follows: the next section describes fundamentals on the proposed actuator. Also, the details on the TSA are outlined in Section 3 and the equations for calculating the relation between the displacement and applied voltage of the TSA are derived in Section 4. The simulation and experimental results are illustrated in Section 5.

Manuscript received December 20, 2007; accepted August 5, 2008. Recommended by Editorial Board member Seung-Hi Lee under the direction of Editor Jae-Bok Song. This research was performed for the Intelligent Robotics Development, one of the 21st Century Frontier R&D Programs is funded by the Ministry of Science and Technology of Korea. We also appreciate the project and equipment support from the Gyeonggi Province through the GRRC program in Sungkyunkwan University.

Nguyen Huu Chuc, Ja Choon Koo, and Hyouk Ryeol Choi are with Department of Mechanical Engineering, Sungkyunkwan University, Chunchon-dong 300, Jangan-gu, Suwon, Korea, 440-746 (e-mails: {chucnh, jckoo, hrchoi}@me.skku.ac.kr).

Young Kwan Lee is with Department of Chemical Engineering, Sungkyunkwan University, Chunchon-dong 300, Jangan-gu, Suwon, Korea, 440-746 (e-mail: yklee@skku.edu).

Jae Do Nam is with Polymer System Engineering, Sungkyunkwan University, Chunchon-dong 300, Jangan-gu, Suwon, Korea, 440-746 (e-mail: jdnam@skku.edu).

* Corresponding author.

Finally, conclusions with future works are given in Section 6.

2. ACTUATION PRINCIPLES

The operational principle of the dielectric elastomer elaborated in previous reports, is briefly introduced in this section [1-3]. When a voltage is supplied across a dielectric elastomer film coated with compliant electrodes on both sides, the film shrinks in thickness and expands in area accordingly, as is shown in Fig. 1. It is a kind of field-induced deformation and the electrostatic force induced by the charges on the surface of the film, called the Maxwell stress, causes contraction of the film along the thickness direction. Based on the simple electrostatic model, the effective pressure can be derived as follows [2]:

$$p = \varepsilon_0 \varepsilon_r \left(\frac{V}{d} \right)^2 , \quad (1)$$

where p is electrostatic pressure (Maxwell stress), and ε_0, ε_r are the free-space permittivity (8.85×10^{-12} F/m) and the relative dielectric constant of the elastomer, respectively. V denotes the applied voltage and d is the thickness of the film.

In general, dielectric elastomer actuators contain two distinguishable regions, known as the *active region* and *nonactive region*, as is shown in Fig. 2. The active region denotes the area covered with the electrode and under the influence of the electric field. The non-active region corresponds to the bare elastomer substrate not covered with the electrode. It is a prerequisite to avoid electrical shortage on the boundary of the dielectric elastomer actuator. However, the non-active region should be minimized to improve the actuation performance since it hampers the deformation of the elastomer.

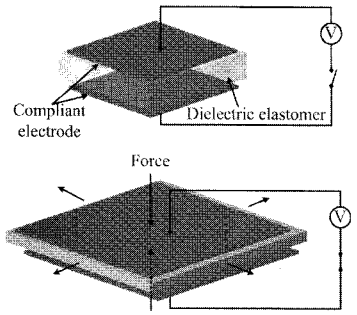

Fig. 1. Operational principle of the dielectric elastomer actuator.

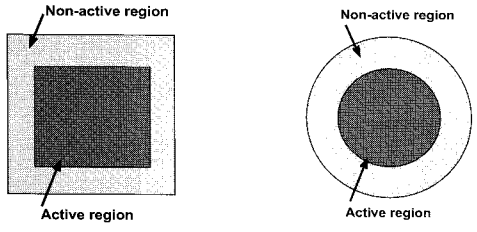

Fig. 2. Active and non-active region.

3. DESIGN OF THE ACTUATOR

The proposed actuator does not have a non-active region along the circumferential direction because it is simply a tube coated with an electrode inside and outside. Thus, the deformation of the active region along the axial direction is not obstructed in the proposed design of the actuator. This is the unique feature that is advantageous over the other actuators reported up to now [4].

As is shown in Fig. 3, a TSA consists of a synthetic elastomer tube, spring and caps with wirings. A spring compressed along the axial direction is inserted inside the tube. The tube is coated with the carbon electrode both inside and outside, as is illustrated in Fig. 4. The inner and outer layers are compliant electrode layers embedded on the surface of the tube, and the synthetic elastomer substrate is between them. Both ends of the tube are terminated with a rigid cap and electrical connections (live, ground). The spring is adopted to enhance the axial deformation while constraining it radially. The design of the TSA can easily be extended to the case of multiple tubes, simply called N-TSA. For instance, the case of 3 layers of tubes is as shown in Fig. 4.

In the case of robotic applications, the N-TSA is useful because it helps us increase the force of the actuator. In fact, the TSA is called 1-TSA because it consists of a synthetic elastomer tube and a compressed spring, as is shown in Fig. 3. The TSA inserted into the other synthetic elastomer tube results in the 2-TSA. Likewise, if N is the number of tubes, N-TSA is made, as is depicted in Fig. 5. As is described in Fig. 5(a), the outer electrode of tube 1 has

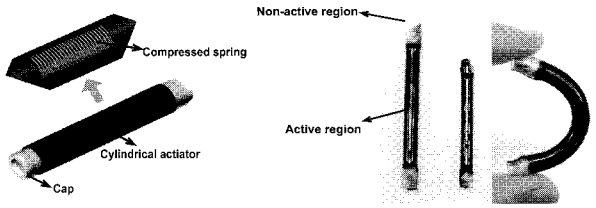

Fig. 3. Tube-Spring Actuator (TSA).

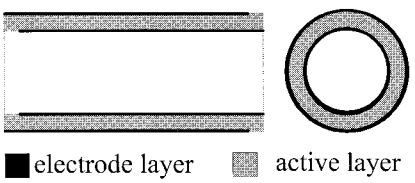

Fig. 4. Cross-sectional view of TSA.

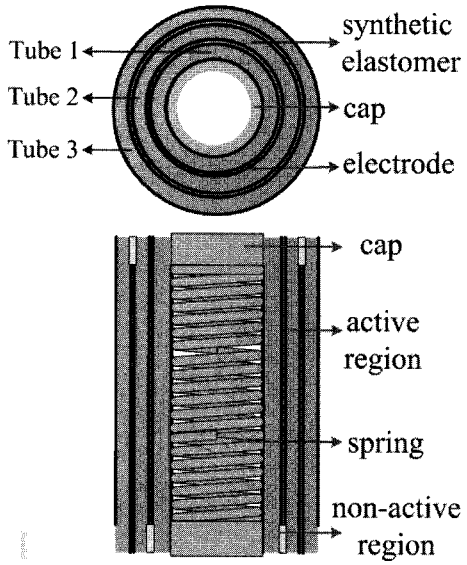

(a) Cross-sectional view of the 3-TSA.

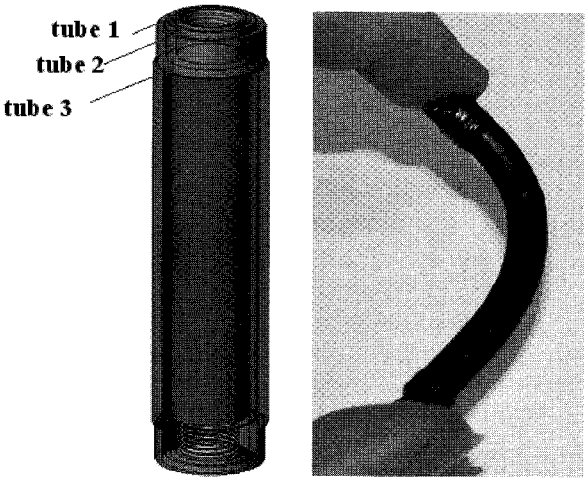

(b) 3-TSA.

Fig. 5. Details of the 3-TSA.

contact with the inner electrode of tube 2. Hence, this contact provides the same voltage potential on both sides. Similarly, the outer electrode of tube 2 is connected to the inner electrode of tube 3. Then, the outer layer of N-TSA is the value of N. Consequently, N-TSA includes N tubes sandwiched alternately among electrode layers. N-TSA is fabricated by using the synthetic elastomer, as is displayed in Fig. 5(b) [11].

The operation of the actuator is simply explained as follows: in its free state, the actuator is under prestrain along the radial as well as the axial direction because the compressed spring is inserted, though no input voltage is given. Typically, the prestrain along the radial direction is relatively small compared to that of the axial one. That is, the actuator is under the dominant prestrain along the axial direction of the coil spring, which makes the tube deform more easily along in the axial direction. The actuator just extends along the axial direction, and when the voltage is applied it produces rectilinear motion.

4. MODELING AND ANALYSIS

The model of the actuator is derived as follows: first, a static model is built up under the linear elasticity theory. Beginning with the model of the TSA, the generalized model the N-TSA is derived. The dynamic model includes both mechanical and electrical behavior of the actuator. The complete model is built up by incorporating both the static model and the dynamic models.

4.1. Static model TSA

Initially, it is assumed that the TSA does not extend over the elastic limit of the synthetic elastomer. The linear elasticity theory can typically be applied if the strain is bounded to less than 20% [2]. When the cylindrical actuator is applied with a driving voltage V, as is shown in Fig. 6, the stress along the thickness direction is derived as follows [9]:

$$p_e = \sqrt{2}\varepsilon_o\varepsilon_r\left(\frac{V}{t}\right)^2, \tag{2}$$

where t is the thickness of the tube ($t << r_0$). As is shown in Fig. 7, the spring has an initial length L_s and its radius is R. Then, it is assumed that the spring is compressed and inserted in the tube whose initial active length, radius and wall-thickness are L_0, R_0 and t_0, respectively. When the spring is inserted inside the tube actuator and both ends of the spring are kept in the tube, the active length L of the TSA is assumed to be larger by ΔL compared to the initial length L_0. F_{sping} and F_{load} represent the forces by the compressed spring and the external load, respectively.

Before applying the voltage, the synthetic elastomer tube is under the influence of two kinds of stresses, namely the circumferential stress due to $R > R_0$ and the axial one due to the F_{sping} and F_{load}. Hence, Hooke's law gives us:

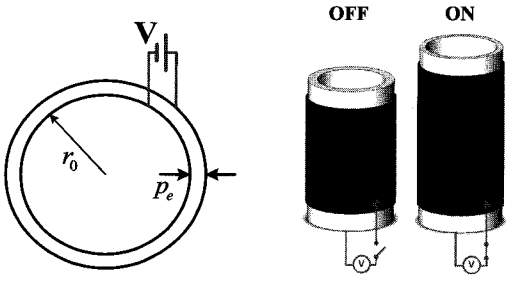

Fig. 6. Operational principle of the cylindrical actuator.

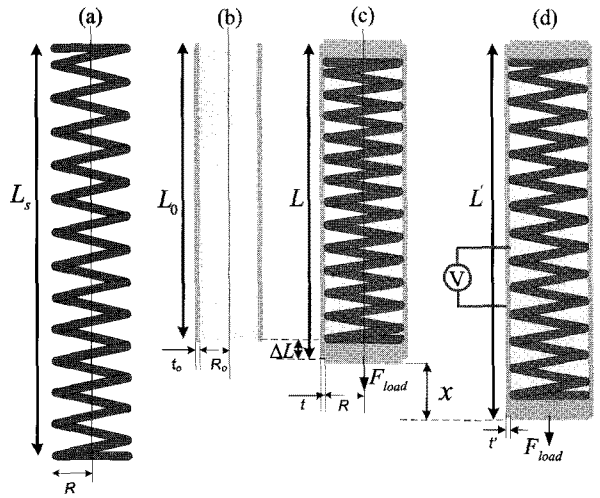

Fig. 7. (a) Initial spring (b) Tube actuator (c) TSA before applying voltage (d) TSA after applying voltage.

$$S_\theta = \frac{1}{E}(\sigma_\theta - \nu\sigma_z), \tag{3}$$

$$S_z = \frac{1}{E}(\sigma_z - \nu\sigma_\theta), \tag{4}$$

where E and ν denote the Young's modulus, and Poisson's ratio, respectively. S_θ is defined as follows:

$$S_\theta = \frac{R - R_0}{R_0} = \zeta - 1, \tag{5}$$

where $\zeta = R/R_0$ and S_θ is a strain along the circumferential direction. Also, S_z is calculated as follows:

$$S_z = \frac{L - L_0}{L_0} = \frac{\Delta L}{L_0}, \tag{6}$$

which is the strain along the radial direction. Then, the axial stress is calculated as follows:

$$\sigma_z = \frac{F_{spring} + F_{load}}{\alpha}, \tag{7}$$

where $F_{sping} = k(L_s - L)$ and k represents the stiffness of the spring. α is the cross-sectional area of the tube. Based on (3)-(7), the length of the TSA, L, before applying the voltage is computed by utilizing the following equation:

$$\left(1-\nu^2\right)\sigma_z - \nu E\frac{L - L_0}{L_0} - \nu E(\zeta - 1) = 0. \tag{8}$$

Let us assume that the displacement of the TSA is x when the driving voltage is given. Then, the extension ratio along the axial direction is computed as follows:

$$\lambda = \frac{L_0 + \Delta L + x}{L_0}. \tag{9}$$

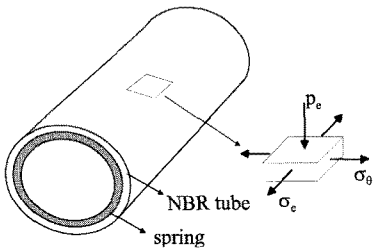

Fig. 8. Stress analysis of the TSA when the voltage is applied.

The thickness of the tube t' and the cross-sectional area of the tube α' are calculated as follows:

$$\begin{aligned}\alpha' &= 2\pi\left[(R+t')^2 - R^2\right] \\ &= \frac{2\pi}{\lambda}\left[(R+t_0)^2 - R^2\right]\end{aligned} \tag{10}$$

and we have:

$$\begin{aligned}t' &= \left[\frac{L_0}{L_0 + \Delta L + x}\left((R_0 + t_0)^2 - R_0^2\right) + R^2\right]^{1/2} - R \\ &= \left[\frac{1}{\lambda}\left((R_0 + t_0)^2 - R_0^2\right) + R^2\right]^{1/2} - R.\end{aligned} \tag{11}$$

Also, the force generated by the spring is calculated as follows:

$$F_{spring} = k\left(L_s - L_0 - \Delta L - x\right) = k\left(L_s - \lambda L_0\right). \tag{12}$$

Similarly, when the voltage is applied, the TSA is under the influence of three stresses, which are the prestress σ'_θ (circumferential stress) in the hoop direction, Maxwell stress p_e, as is given in (2) in the radial direction and axial stress σ'_z by the spring and the load calculated from $\sigma'_z = \left(F_{load} + F_{spring}\right)/\alpha'$. Hooke's law provides:

$$S'_\theta = \frac{1}{E}\left[\sigma'_\theta - \nu\left(-p_e + \sigma'_z\right)\right], \tag{13}$$

$$S'_z = \frac{1}{E}\left[\sigma'_z - \nu\left(\sigma'_\theta - p_e\right)\right], \tag{14}$$

where $S'_\theta = \zeta - 1$ and $S'_z = \left(x + \Delta L\right)/L_0$ are the strain along circumferential and axial directions, respectively. Multiplying (13) with ν and adding to (14) yields:

$$\left(1-\nu^2\right)\sigma'_z + \nu(1+\nu)p_e - ES'_z - \nu ES'_\theta = 0. \tag{15}$$

After multiplying with α', (15) becomes:

$$\begin{aligned}&\underbrace{\left(1-\nu^2\right)\left(F_{load} + F_{spring}\right)}_{axial\ force} + \underbrace{\alpha'\nu(1+\nu)p_e}_{Maxwell\ force} \\ &- \underbrace{\alpha' ES'}_{elastic\ force} - \underbrace{\alpha'\nu E(\zeta - 1)}_{prestrain\ force} = 0.\end{aligned} \tag{16}$$

Equation (16) consists of four groups of terms: group 1 is the force by spring and external load, group 2 is the force caused by the Maxwell stress, group 3 is the force caused by the elastic restoration force of the synthetic elastomer and group 4 is the force caused by the prestrain. When the TSA is given with the input voltage, the displacement x can be calculated by utilizing (16). The output force of the TSA along the axial direction is calculated as described in (17) when $F_{load} = 0$ and $x = 0$.

$$F_{TSA_{output}} = \alpha'_{x=0}\nu(1+\nu)\sqrt{2}\varepsilon_0\varepsilon_r\left(\frac{V}{t'_{x=0}}\right)^2 \tag{17}$$

4.2. Generalized static model of the N-TSA

The model of the N-TSA can be obtained by generalizing that of the TSA. Because the electrode layer is compliant and its thickness is very small compared to the tube thickness, the thickness of the electrode layer is negligible. Without loss of generality, it is assumed that the deformation of each tube in the N-TSA is similar to that described in Fig. 9. Therefore, the Maxwell stress in duced on each tube is the same as in the first tube. Applying (16) to the tube i yields:

$$\begin{aligned}&\left(1-\nu^2\right)\left(F_{load}+F_{spring}\right)+\alpha'_i\nu(1+\nu)p_e\\&\quad-\alpha'_iES'-\alpha'_i\nu E\left(\zeta-1\right)=0.\end{aligned} \tag{18}$$

In (18), ζ is assumed to be similar in each tube. By applying this equation for each tube when i changes from 1 to N, we have:

$$\begin{aligned}&N\left(1-\nu^2\right)\left(F_{load}+F_{spring}\right)+\sum_{i=1}^{N}\alpha'_i\nu(1+\nu)p_e\\&\quad-\sum_{i=1}^{N}\alpha'_iES'-\sum_{i=1}^{N}\alpha'_i\nu E\left(\zeta-1\right)=0.\end{aligned} \tag{19}$$

Without loss of generality, assuming that $\sum_{i=1}^{N}\alpha'_i \approx N\alpha'_1$, (19) is written by

$$\begin{aligned}&N\left[\left(1-\nu^2\right)\left(F_{load}+F_{spring}\right)+\alpha'_1\nu(1+\nu)p_e\right.\\&\quad\left.-\alpha'_1ES'_z-\alpha'_1\nu E\left(\zeta-1\right)\right]=0.\end{aligned} \tag{20}$$

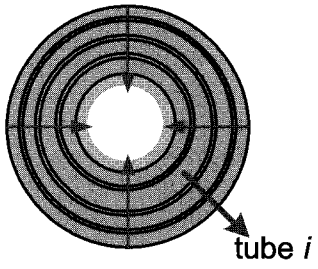

Fig. 9. The direction of the deformation of each tube when the driving voltage is applied.

Comparing (20) with the (16), the displacement of the N-TSA shows the same displacement x with the TSA when the N-TSA and TSA are subjected to the same driving voltage. In addition, the output force of the N-TSA can be calculated as follows:

$$\begin{aligned}F_{N-TSA_{output}} &= N \times F_{TSA_{output}}\\&= N\times\left[\alpha'_{x=0}\nu(1+\nu)\sqrt{2}\varepsilon_0\varepsilon_r\left(\frac{V}{t'_{x=0}}\right)^2\right].\end{aligned} \tag{21}$$

4.3. Dynamic model

Along with the static model previously discussed, a dynamic model can also be derived. In the present work, the dynamic model of the TSA including both the electrical and the mechanical behavior is built [12].

The electrical model of the actuator includes the resistance of the wire R_w, the resistance of the actuator R_e and the capacitance of the actuator C_p connected in series, as is illustrated in Fig. 10. The capacitance of the elastomer tube is calculated as follows:

$$C_p = \frac{2\pi\varepsilon_o\varepsilon_r L'}{\ln\left(1+\frac{r'}{R}\right)}. \tag{22}$$

Assuming $t' \ll R$, (22) can be approximated as follows:

$$C_p \approx \frac{2\pi\varepsilon_r\varepsilon_0 RL_0\lambda}{t'}. \tag{23}$$

Also, we have:

$$v(t) = \left(R_w + R_e\right)i(t) + e_p(t), \tag{24}$$

where $e_p(t)$ is the voltage between two electrodes of the actuator and is calculated as follows:

$$e_p(t) = \frac{1}{C_p}\int i(t) = \frac{q(t)}{C_p}. \tag{25}$$

Using the Laplace transform and combining Eqs. (24) and (25), we have:

$$V(s) = \left(R_w + R_e\right)I(s) + \frac{Q(s)}{C_p}. \tag{26}$$

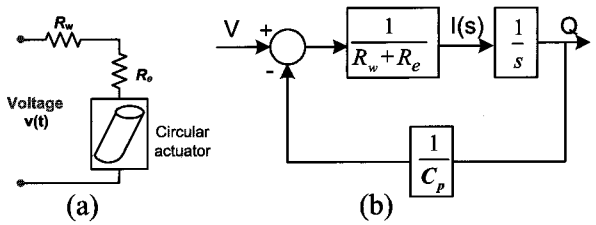

Fig.10. (a) Electrical model of the cylindrical tube (b) Block diagram of the electrical circuit.

Based on (26), the state block diagram for the electrical model of the TSA is represented as Fig. 10 and the charge of the actuator Q and the Maxwell stress can be calculated as follows:

$$p = \sqrt{2}\varepsilon_0\varepsilon_r\left(\frac{E_p}{t'}\right)^2 = \sqrt{2}\varepsilon_0\varepsilon_r\left(\frac{Q}{t'C_p}\right)^2 = \sqrt{2}\varepsilon_0\varepsilon_r\left(\frac{Q}{2\pi L_0 R\lambda}\right)^2. \tag{27}$$

Polymers such as rubbers deform like a flow when they are subjected to external stresses, and they are called viscoelastic because the flow dissipates energy due to an internal loss mechanism [13]. In the case of the viscoelastic material, its elastic modulus Y is not constant during its operation and thus, we have

$$E = E(t) = \frac{\sigma(t)}{\varepsilon(t)}, \tag{28}$$

where $\sigma(t)$ is the stress and $\varepsilon(t)$ is the strain of the dielectric elastomer. The viscoelastic behavior of the material, in general, can be analyzed by introducing finite networks of springs and dashpots, typically either the Maxwell model, Kelvin model, Standard Linear model (three-element model), generalized mechanical model, etc. [13]. In the present work, the extension of the Standard Linear model is used to describe the viscoelastic property of the dielectric elastomer. The proposed model includes five elements, as is shown in Fig. 11.

If $E(t)= 1/J(t)$, where $J(t)$ is the reciprocal of the elastic modulus, the proposed model can be derived by using a Laplace transformation such as

$$J(s) = \frac{\varepsilon(s)}{\sigma(s)} = \frac{1}{E_0} + \frac{1}{k_1 + \eta_1 s} + \frac{1}{k_2 + \eta_2 s}. \tag{29}$$

Consequently, the function of the elastic modulus is defined completely when the parameters of the springs and dashpot are determined. Equation (16) produces the deformation of the TSA in the time domain as follows:

Mechanical model

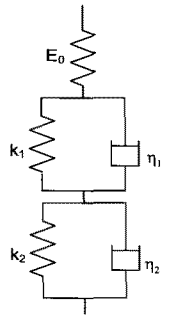

Fig. 11. Viscoelastic model of the actuator.

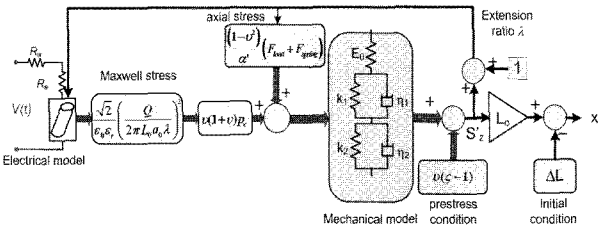

Fig. 12. The complete model of TSA.

$$S_z' = J(t)\left[\left(1-\nu^2\right)\frac{F_{load}+F_{spring}}{\alpha'} + \nu(1+\nu)p_e(t)\right] - \nu(\zeta-1). \tag{30}$$

Thus, the displacement of the TSA can be obtained as follows:

$$x = L_0 S_z' - \Delta L = L_0\left[J(t)\left[\left(1-\nu^2\right)\frac{F_{load}+F_{spring}}{\alpha'} + \nu(1+\nu)p_e\right] - \nu(\zeta-1)\right] - \Delta L. \tag{31}$$

The complete model incorporates the electrical and mechanical model, as is shown in Fig. 12. From (27), the Maxwell stress is defined with the charge Q on the actuator when the driving voltage is applied. The Maxwell stress associated with the external force will become the input stress of the mechanical model. Thus, the output of the mechanical model is the axial strain that modifies both the thickness and cross-sectional area of the tube. The proposed model is useful for predicting the behavior of the TSA as well as for designing the controller for the proposed actuator in the near future.

5. SIMULATION AND EXPERIMENTS

In this section, the proposed model is validated via the simulation and experimental results. The procedures are described in details and the results are then discussed.

5.1. Experimental setup

In the present work, the dimensions of the actuator are given as follows: the inner diameter of the tube is 6.5mm and the thickness of the tube is 165μm. The initial length of the compressed spring, the length of the active region, diameter and stiffness are 200mm, 43mm, 6.8mm and 3N/m, respectively. It is inserted inside the tube and terminated with two plastic caps. After the spring is inserted, the active region length of the TSA becomes 45mm. In addition, a 2-TSA and 3-TSA are also fabricated to be compared with the original TSA. The experimental setup is illustrated in Fig. 13. The displacement of the TSA is measured by

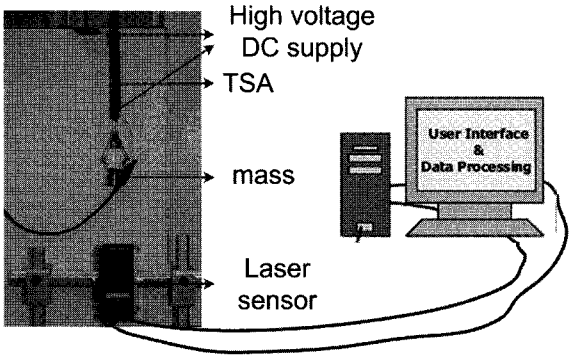

Fig. 13. Experimental setup for measuring the displacement.

using a laser displacement sensor while one side of the TSA is fixed and the other is subjected to a constant load. The actuator is actuated by using a driving circuit that generates different waves of high voltages at variable frequencies.

5.2. Identification of parameters

The viscoelastic model proposed in Section 4.3 of the present work is identified experimentally. The related parameters are estimated by using the response of engineering strain with respect to time, as is shown in Fig. 14. According to the definition, creep corresponds to the slow and continuous strain resulting from the constant stress. Hence, the strain's equation of the proposed model is represented as follows [13]:

$$\varepsilon(t)=\frac{\tau_0}{E_0}+\frac{\tau_0}{k_1}\left[1-e^{-\frac{k_1 t}{\eta_1}}\right]+\frac{\tau_0}{k_2}\left[1-e^{-\frac{k_2 t}{\eta_2}}\right].$$

In practice it always takes a time t_0 to get a constant stress, as is shown in Fig. 14. Consequently, in this paper, *Boltzman's Superposition Principle* is adopted

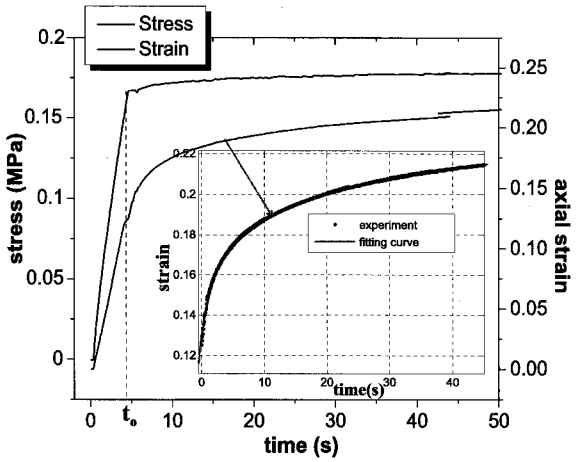

Fig. 14. The creep property of the synthetic elastomer tube under constant stress along with the fitted curve.

Table 1. Estimation of the parameters.

Parameter	Value
$E0(MPa)$	2.9374
$k1(MPa)$	2.9392
$k2(MPa)$	1.7936
$\eta1(MPa.s)$	5.8596
$\eta2(MPa.s)$	3.1943
εr	14
$Rw + Re(K\Omega)$	800
$mass(g)$	10

to determine the strain for $t > t_0$ as follows [13]:

$$\varepsilon(t)=\tau_0\left[\frac{1}{E_0}+\frac{1}{k_1}+\frac{1}{k_2}\right]+\frac{\tau_0\eta_1}{t_0 k_1^{\,2}}\left[1-e^{\frac{k_1 t_0}{\eta_1}}\right]e^{-\frac{k_1 t}{\eta_1}}+\frac{\tau_0\eta_2}{t_0 k_2^{\,2}}\left[1-e^{\frac{k_2 t_0}{\eta_2}}\right]e^{-\frac{k_2 t}{\eta_2}}. \quad (32)$$

Equation (32) represents the strain for $t > t_0 = 4.441$ *s*. However, to conveniently estimate the material parameters from experiments, the strain curve for $t > t_0$ is shifted as much as t_0, as is shown in Fig. 14. Therefore, the engineering strain is rewritten as follows:

$$\varepsilon(t)=\tau_0\left[\frac{1}{E_0}+\frac{1}{k_1}+\frac{1}{k_2}\right]+\frac{\tau_0\eta_1}{t_0 k_1^{\,2}}\left[e^{\frac{k_1 t_0}{\eta_1}}-1\right]e^{-\frac{k_1 t}{\eta_1}}+\frac{\tau_0\eta_2}{t_0 k_2^{\,2}}\left[e^{\frac{k_2 t_0}{\eta_2}}-1\right]e^{-\frac{k_2 t}{\eta_2}}. \quad (33)$$

The material parameters E_0, k_1, k_2, η_1, and η_2 are estimated via curve fitting, and the resistance, mass (load) dielectric constant are determined as given in Table 1.

5.3. Results and discussions

Initially, the response of the TSA is compared with that of the simulation upon the square input voltage, as is shown in Fig. 15. The displacement of the TSA increases for 34 seconds and then decreases. The simulation result is similar to this experimental result. The simulation and experimental result both show slow saturation, which can be explained in two ways. Firstly, the synthetic elastomer has some viscoelastic properties [11] that make the output displacement respond slowly. Secondly, the compressed spring has a tendency to return to the original state, hence, that makes the output displacement be in low saturation. This is the shortcoming of the dielectric elastomer actuator using the compressed spring.

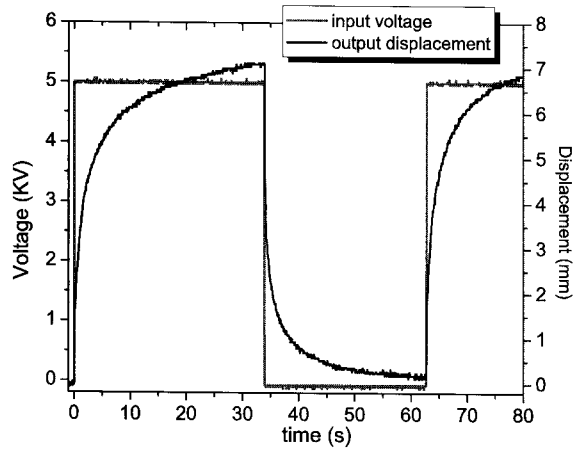

(a) experiment.

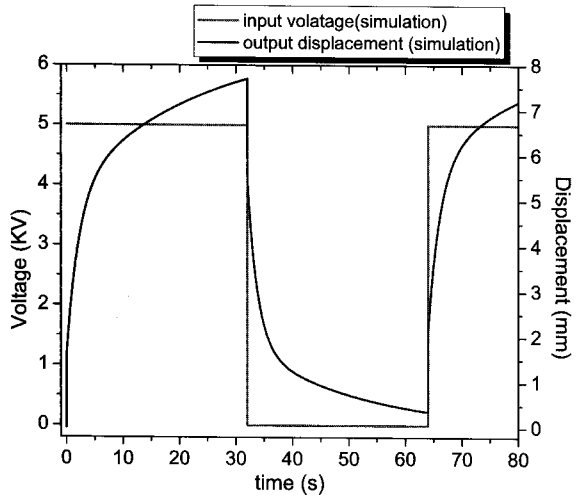

(b) simulation.

Fig. 15. The displacement of the TSA on square input voltages.

The displacement of the TSA, 2-TSA and 3-TSA are also compared when a square input voltage, whose frequency is 0.1 Hz, is given. As is shown in Fig. 16, the displacements of the three actuators are almost the same. The deformation of the proposed model is also in good accordance with that of N-TSA with respect to the input voltage. However, some differences exist among the deformations of the TSA, 2-TSA, 3-TSA and the simulation result due to the non uniformity of the tubes when they are manufactured.

In addition, the frequency response of TSA is verified as shown in Fig. 17. The displacement of the actuator is measured when the input voltage is kept at 4.5 KV and the frequency varies from 0.1 Hz to 10 Hz. According to these experimental results, when the frequency increases, the displacement of the actuator decreases. This result indicates the limited applicability of the proposed actuator for high speed applications (> 10 Hz).

Finally, to compare the *N*-TSA with the TSA, the output forces of these actuators are measured with a force sensor. The TSA, 2-TSA and 3-TSA are

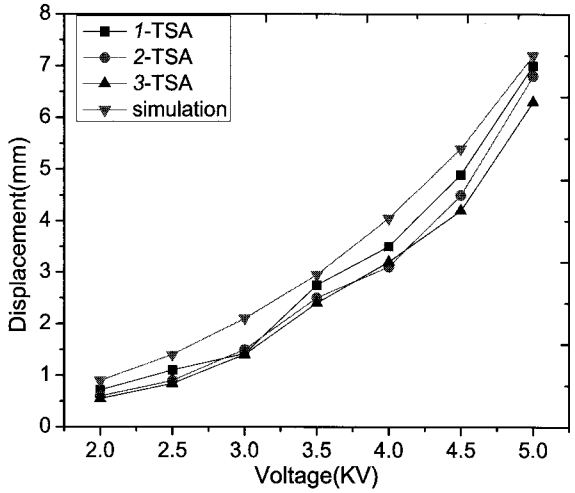

Fig. 16. The output displacement of the N-TSA.

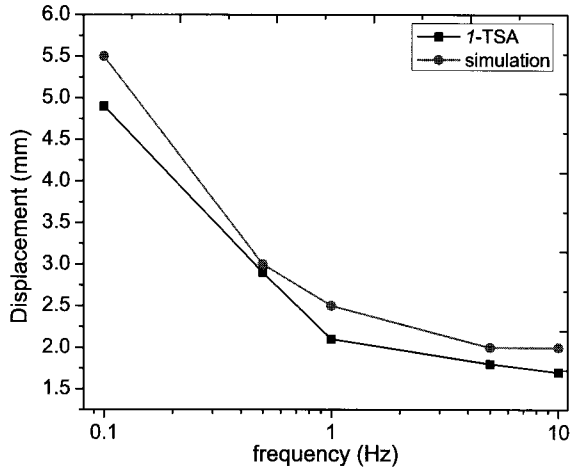

Fig. 17. The displacement with respect to frequency of the TSA.

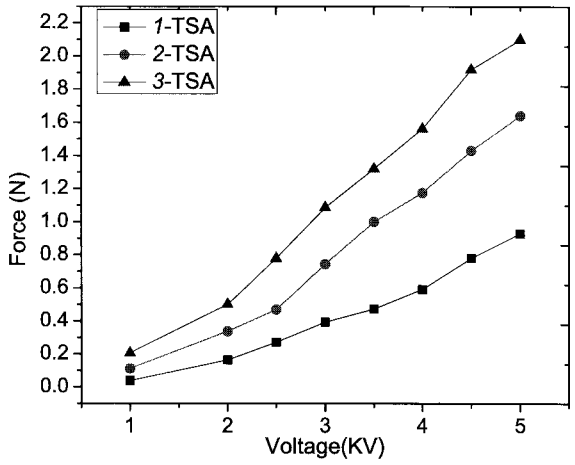

Fig. 18. The output force of the N-TSA.

measured by being held in place when a driving voltage is applied. The results are shown in Fig. 18 and explain that the output force of the 2-TSA is nearly double that of the TSA, and the 3-TSA is approximately three times that of the TSA. Therefore,

N (number of the tube) can be determined to adapt the desired force based on the requirements of the application.

6. CONCLUSIONS

This paper introduces a tube-like artificial muscle actuator. The advantages of this actuator are that the non-active region does not affect to the deformation of the active region. Moreover, the proposed actuator is easy to fabricate and competitive in its unit cost. The model that integrates the electrical and mechanical models is developed and its feasibility is proved via simulation and experimental results. The actuator still has the limitation of a slow response due to creep and from its structural flexibility. This problem is being investigated, and it can be improved by introducing dedicated driving circuitry [1]. Additionally, the applicability of the proposed actuator to high speed application needs to be improved in the future, while the future techniques for controlling the actuator will help us get better performance out of the actuator.

REFERENCES

[1] K. J. Kim and S. Tadokoro, *Electroactive Polymer for Robotic Applications*, Springer, 2007.

[2] R. Pelrine, R. Kornbluh, and J. Joseph, "Electrostriction of polymer dielectrics with compliant electrodes as a means of actuation," *Sensors and Actuators A*, vol. 64, pp. 77-85, 1998.

[3] R. Pelrine, R. Kornbluh, Q. Pei, and J. Joseph, "High-speed electrically actuated elastomer with strain greater than 100%," *Science*, vol. 287, pp. 836-839, 2000.

[4] R. Pelrine, R. Kornbluh, Q. Pei, J. Joseph, and M. Rosenthal, "Electroelastomer rolls and their application for biomimetic walking robots," *Synthetic Metal*, vol. 135, pp. 129-131, 2003.

[5] F. Carpi, A. Migliore, and D. Rossi, "A new contractile linear actuator made of dielectric elastomers," *Proc. SPIE. on Smart Structures and Materials: Electroactive Polymer Actuators and Devices (EAPAD)*, vol. 5759, pp. 64-74, 2005.

[6] J. C. Koo, K. M. Jung, J. K. Park, J. Nam, Y. K. Lee, J. W. Jeon, and H. R. Choi, "Representation of a conceptual design for a rectilinear motion polymer actuator," *International Journal of Control, Automation and Systems*, vol. 5, no. 4, pp. 429-435, 2007.

[7] H. R. Choi, K. M. Jung, S. M. Ryew, J. D. Nam, J. W. Jeon, J. C. Koo, and K. Tanie, "Biomimetic Soft Actuator: Design, Modelling, Control and Applications," *IEEE/ASME Trans. on Mechatronics*, vol. 10, no. 5, pp. 581-593, 2005.

[8] M. Y. Jung, K. M. Jung, N. H. Chuc, I. M. Koo, J C. Koo, Y. K. Lee, J. D. Nam, and H. R. Choi, "Fabrication and characterization of linear motion dielectric elastomer actuators," *Proc. SPIE. on Smart Structures and Materials: Electroactive Polymer Actuators and Devices (EAPAD)*, vol. 6168, pp. 6168241-7, 2006

[9] A. Rajamani, M. Grissom, C. Rahn, Y. Ma, and Q. Zhang, "Wound roll dielectric elastomer actuators: Fabrication, analysis and experiments," *Proc. of IEEE/RSJ International Conference on Intelligent Robots and Systems*, pp. 1520-1525, 2005.

[10] A. Wingert, M. D. Lichter, and S. Dubowsky, "On the design of large degree-of-freedom digital mechatronic devices based on bistable dielectric elastomer actuators," *IEEE/ASME Trans. on Mechatronics*, vol. 11, no. 4, pp. 448-456, 2006.

[11] K. M. Jung, J. H. Lee, M. S. Cho, J. C. Koo, J. D. Nam, Y. K. Lee, and H. R. Choi, "Development of enhanced synthetic elastomer for the energy efficient polymer actuators," *Smart Materials and Structures*, vol. 16, pp. S288-S294, 2007.

[12] C. M. Hackl, H. Y. Tang, R. D. Lorenz, L. S. Turng, and D. Schroder, "A Multidomain model of planar electro-active Polymer Actuators," *IEEE Trans. on Industry Application*, vol. 41, no. 5, pp. 1142-1148, 2005.

[13] Y. M. Haddad, *Viscoelasticity of Engineering Material*, Chapman & Hall, 1995.

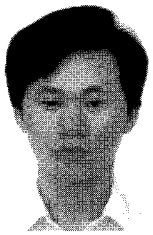

Nguyen Huu Chuc received the B.S. degree in Electrical Engineering from the HCM University of Technology, Vietnam in 2003. He is currently working toward a Ph.D. degree in Mechanical Engineering from Sungkyunkwan University, Intelligent Robotics and Mechatronic System Laboratory (IRMS lab). His research interests include artificial muscle actuators and control.

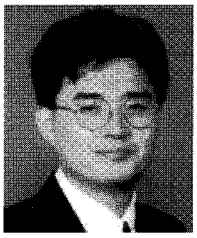

Ja Choon Koo was born in Seoul Korea and educated in both Seoul and Austin. He received the Ph.D. and M.S. degree from the University of Texas at Austin, in 1997 and 1992, respectively and the B.S. degree from Hanyang University, in 1989. He is an Assistant Professor in the School of Mechanical Engineering at Sungkyunkwan University in Korea. He was an Advisory Engineer for IBM, San Jose, CA, and a Staff Engineer for Samsung Information Systems America, San Jose, CA. His research interests are modeling of dynamics systems, sensors and actuators.

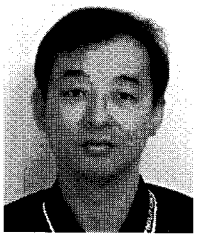

Jae Do Nam received the B.S. and M.S. degrees in Chemical Engineering from Seoul National University in 1994 and 1986, respectively. In 1991, he received the Ph.D. degree in Chemical Engineering at the University of Washington, Seattle, WA. He is a Professor in the Department of Polymer Science and Engineering, Sungkyunkwan University, Suwon, Korea. He worked at the Polymeric Composites Laboratory, University of Washington, as a Research Associate from 1991 to 1993. Returning to Korea, he joined Jeil Synthetic Fiber Co., Samsung Group, in 1993-1994, and moved to Sunkyunkwan University in 1994. He is actively working in the areas of polymer sensors and actuators, organic/inorganic nanocomposites, biodegradable polymers and compo-sites, and nanoparticles and nanoporous structure. He has published over 70 technical papers.

Young Kwan Lee received the B.S. degree in Chemical Engineering from Sungkyunkwan University in 1982. He received the M.S. and Ph.D. degrees in Polymer Engineering at the University of Southern Mississippi in 1987 and 1991, respectively. He is a Professor in the Department of Chemical Engineering, Sungkyunkwan University, Korea. From 1984 to 1986, he worked at LG Chemical in Research. He stayed at the Polymer Research Institute, University of Florida, as a Research Associate in 1992. From 1992 to 1993, he worked at Coating Resin Div., Reichhold Chem. in NC, USA, as a Researcher. Returning to Korea in 1993, he joined the faculty of Chemical Engineering, Sungkyunkwan University and currently is a Professor. From 1997 to 1998, he worked at The Polymer Society of Korea as an editor. From 1998 to 2000, he has been the Director of the Polymer Technology Institute in Sungkyunkwan University, Korea. From 1999 to 2001, he has been the councilor for the Korean Institute of Chemical Engineers. From 2001 to 2002, he worked at the University of Florida, as a Visitation Researcher. His interests include actively working in the areas of polymer sensors and actuators, conducting polymers, fuel cells, biodegradables and composites, etc.

Hyouk Ryeol Choi received the B.S. degree from Seoul National University, Seoul, Korea, in 1984, the M.S. degree from the Korea Advanced Institute of Science and Technology (KAIST), Taejon, Korea, in 1986, and the Ph.D. degree from the Pohang University of Science and Technology (POSTECH), Pohang, Korea, in 1994. Since 1995, he has been with Sungkyunkwan University, Suwon, Korea, where he is currently a Professor in the School of Mechanical Engineering. He was an Associate Engineer with LG Electronics Central Research Laboratory, Seoul, Korea, from 1986 to 1989. From 1993 to 1995, he was with Kyoto University, Kyoto, Japan, as a grantee of scholarship funds from the Japanese Educational Administry. He visited the Advanced Institute of Industrial Science Technology (AIST), Tsukuba, Japan, as a JSPS Fellow from 1999 to 2000. His interests include dextrous mechanisms, field application of robots, and artificial muscle actuators.